High Efficiency Photodetection Below the Quantum Noise Limit

by

Elizabeth Caryn Bullard

Submitted to the Department of Physics
in partial fulfillment of the requirements for the degree of

Bachelor of Science

at the

MASSACHUSETTS INSTITUTE OF TECHNOLOGY

June 2005

Author .....
Department of Physics
May 6, 2005

Certified by .....
Professor Nergis Mavalvala
Assistant Professor of Physics
Thesis Supervisor

Accepted by .....
Professor David E. Pritchard
Senior Thesis Coordinator, Department of Physics

High Efficiency Photodetection Below the Quantum Noise Limit

by

Elizabeth Caryn Bullard

Submitted to the Department of Physics
on May 6, 2005, in partial fulfillment of the
requirements for the degree of
Bachelor of Science

Abstract

Two low-noise, high quantum efficiency, high bandwidth photodetectors have constructed to form a balanced homodyne detector to detect squeezed light. The detectors have quantum efficiencies of 85% and 90%, a bandwidth of 1MHz, and a dark noise of $4.4 \times 10^{-9} \frac{V}{\sqrt{Hz}}$ at 1MHz.

Thesis Supervisor: Professor Nergis Mavalvala
Title: Assistant Professor of Physics

Acknowledgments

I would like to thank Professor Nergis Mavalvala, Eugeniy Mikhailov, Keisuke Goda, and Jon Allen for their help with my thesis project.

Contents

List of Figures

List of Tables

Introduction

LIGO, the Laser Interferometer Gravitational-Wave Observatory [1], is comprised of two detectors; the goal of LIGO is to measure gravitational waves from astrophysical sources such as black holes, neutron stars, and supernovae. Each LIGO detector consists of a power recycled Michelson interferometer with four kilometer long arms. The interferometers are so large due to the sensitivity requirements; a strain sensitivity of at least 10^{21} is required to detect gravitational waves from a pair of inspiralling neutron stars located 15 MPc from Earth. The sensitivity of the current interferometers is limited by noise sources such as seismic noise at low frequencies (under 70Hz), thermal noise from the test masses in 70Hz-200Hz band, and shot noise at higher frequencies, the 200Hz-10KHz band.

Research is currently underway for a more sensitive version of LIGO, Advanced LIGO. In this setup, the noise in the interferometers will be dominated by quantum noise, due to improvements in seismic noise reduction and suppression of thermal noise. Quantum noise arises from the Heisenberg uncertainty principle; quantum noise manifests itself as both shot noise and radiation pressure noise.

The MIT LIGO quantum measurement group is currently researching experimental setups that will reduce shot noise in the 200Hz-10KHz detection band through the injection of squeezed light into the antisymmetric port of the LIGO interferometers[5]. Currently, we are developing techniques to produce squeezed light in the relevant frequency range. A key part of the experiment is the photodetectors used for the detection of the squeezed light. However, commercial photodetectors do not meet the stringent requirements for photodetectors in a squeezing experiment; the photodetectors must have a high quantum efficiency of 90% while remaining shot noise limited.

We designed, built, and tested photodetectors that met these stringent requirements for the detection of squeezed light.

Overview

In Chapter 1, we discuss quantum noise and possible methods to reduce quantum noise in the detection band. In Chapter 2, we give an overview of the squeezing experiment and the homodyne detection system. In Chapter 3, we discuss the limitations considered in the design process and explain how the detectors work. In Chapter 4, we describe the experimental setup and demonstrate the improvement in squeezing detection due to the new photodetectors. Finally, in Chapter 5, we present some conclusions.

Chapter 1

Quantum Noise

The sensitivity of the LIGO detectors is currently limited by seismic noise at low frequencies and thermal noise at high frequencies. However, future versions of LIGO will be limited by quantum noise[5].

1.1 Overview of LIGO Interferometer

Before discussing the sources of quantum noise in the LIGO interferometer, we will give an overview of the instrument and how it detects gravitational waves [1]. The LIGO interferometer is a Michelson interferometer with a power recycling cavity, as shown in Figure 1-1. Each arm of the interferometer contains a Fabry-Perot cavity; the length of the cavity is set by the separation between the test masses, which serve as the mirrors in the Fabry-Perot cavity. LIGO detects gravitational waves by measuring differential changes in the length of the arm cavities. A passing gravitational wave would shorten the length of one arm while lengthening the other. The changing lengths of the cavities lead to changes in phase, as shown by Eq. 1.1,

$$\delta\phi = \frac{4\pi\Delta L N}{\lambda} \tag{1.1}$$

where λ is the frequency of the light, ΔL is the change in length of the cavity, and N is the number of bounces in the cavity[2]. Due to the noise considerations discussed in

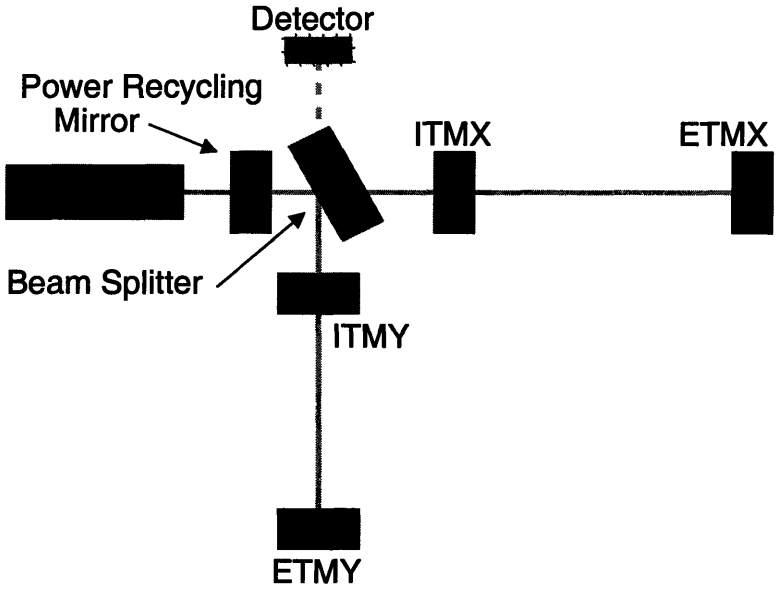

Figure 1-1 Simplified diagram of the LIGO interferometer. ITMX, ITMY, ETMX, and ETMY are all test masses.

Section 1.2, the phase detectors are located at the antisymmetric of the beamsplitter, which is kept on a dark fringe.

1.2 Origins of Quantum Noise

Quantum noise arises from the Heisenberg uncertainty principle. The two sources of quantum noise in an interferometer are shot noise and radiation pressure. Shot noise is the fluctuation in the flux of photons in the output port. Radiation pressure is fluctuations in the position of the test masses due to fluctuations in the number of photons hitting the mirror. Radiation pressure gives a particle an unknown momentum during the first measurement of the particle's position; when one attempts to measure the position of the particle again, the accuracy of the measurement is limited by the unknown momentum.

If the interferometer is operated on a dark fringe[1], where the interferometer has the highest signal to noise ratio, the quantum noise fluctuations in photon fluctuations

[1]See [2] for a full derivation of the quantum noise in an interferometer

are given by Eq. 1.2

$$\delta\phi_{QNL} = \frac{1}{\sqrt{N_{in}\tau}} \tag{1.2}$$

where N_{in} is the number of photons that pass in front of the detector in a time interval τ. The phase noise due to motion of the test masses is given by Eq. 1.3.

$$\delta\phi_{RP} = \frac{\hbar}{m\Omega^2\lambda^2}\sqrt{N_{in}\tau} \tag{1.3}$$

where m is the mass of the test masses, λ is the wavelength of the incident light, and Ω is the frequency at which the fluctuations occur. Unlike shot noise, the radiation pressure is frequency dependent; it is most prominent at lower frequencies due to its $\frac{1}{f^2}$ dependence. These two noise sources can be combined to give the total quantum noise present in the interferometer.

$$\delta\phi_{QM}^2 = \delta\phi_{QNL}^2 + \delta\phi_{RP}^2 \tag{1.4a}$$

$$\delta\phi_{QM}^2 = \frac{1}{N_{in}\tau} + \frac{\hbar^2 N_{in}\tau}{m^2\Omega^4\lambda^4} \tag{1.4b}$$

The total quantum noise can be improved by increasing both the mass of the test masses and by increasing the power of the laser. Both of these methods will be implemented in future versions of LIGO [7].

However, the quantum noise cannot go below the standard quantum noise limit, (SQL), where the uncertainty in the position measurement due to shot noise is equal to the uncertainty in the position measurement to radiation pressure without employing further techniques to reduce quantum noise [5]. Before discussing theses techniques to make measurements below the SQL, it is useful to change the paradigm used to describe shot noise and radiation pressure. Instead of describing them as momentum and position, they can be described as fluctuations in the amplitude quadrature of the input vacuum at the dark port and fluctuations in the phase quadrature of the input vacuum at the dark port.

1.3 Techniques to Reduce Quantum Noise

The MIT LIGO quantum measurement group is currently investigating the injection of vacuum squeezed light into the unused used port of a gravitational wave interferometer as a method to make measurements below the QNL limit. The squeezed light increases the fluctuations in one quadrature quadrature and reduces the fluctuations in the other quadrature. Squeezed light will reduce the noise by a factor of e^{-2R}, the power squeeze factor. In addition, the squeeze angle determines the amount of squeezing that occurs in each quadrature. Figure 1-2 demonstrates the predicted noise improvement in the detection band due to the use of squeezing. Thus, the use of

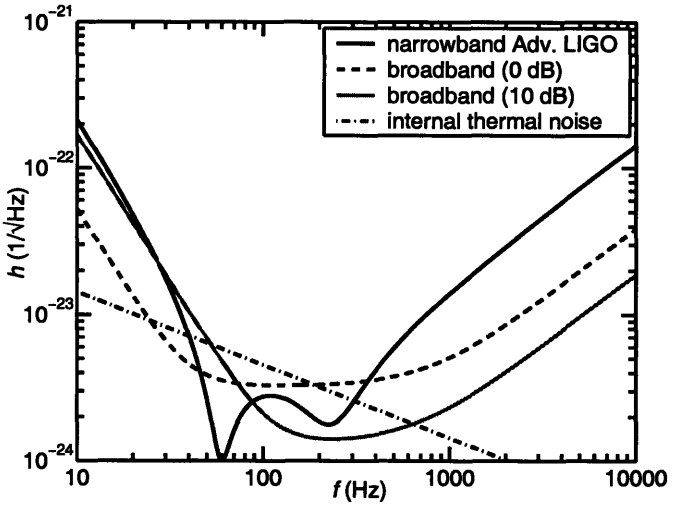

Figure 1-2 Noise curves for Advanced LIGO with different levels of squeezing. The blue line gives the baseline sensitivity of Advance LIGO when limited by quantum noise. The dashed purple line gives the sensitivity for an interferometer configured for squeezing, but with no squeezed input. The solid green line gives the sensitivity for a broadband configuration with 10dB of squeezed input. The dashed-dot brown line gives an estimate of the thermal noise present. Taken from[5].

squeezed input into the unused port of the interferometer can lead to measurements below the SQL.

Chapter 2

Generation and Detection of Vacuum Squeezed Light

The LIGO quantum measurement at MIT is currently building sources of squeezed vacuum for injection into the dark port of a gravitational wave interferometer. Figure 2 [4] demonstrates a possible setup for the table top experiment currently in development. The Diabolo Laser generates green light at 532nm (the green line on the diagram) and infrared light at 1064 nm (the red line on the diagram). The squeezer generates squeezed vacuum at 1064nm (the dashed red line) using an optical parametric oscillator (OPO). The squeezed light is then injected into the dark port of the power-recycled Michelson interferometer. The output of the power-recycled Michelson interferometer is detected at the homodyne detector. Alternatively, the squeezed light can be directly measured using homodyne detecXtion.

2.1 Generation of Squeezed Light

An optical parametric oscillator is used to create squeezing[8],[12]. The OPO cavity is composed of a crystal with a $\chi^{(2)}$ nonlinearity housed inside of an oven; the temperature of the crystal controls the phase matching condition. The OPO is pumped by light at 532 nm. The photons interact with the crystal and are down converted to form 2 photons at 1064. The Hamiltonian of this system is given by Eq. 2.1, where

Squeezed-Vacuum-Injected Power-Recycled Michelson Interferometer
Conceptual Design (Version 3.2)

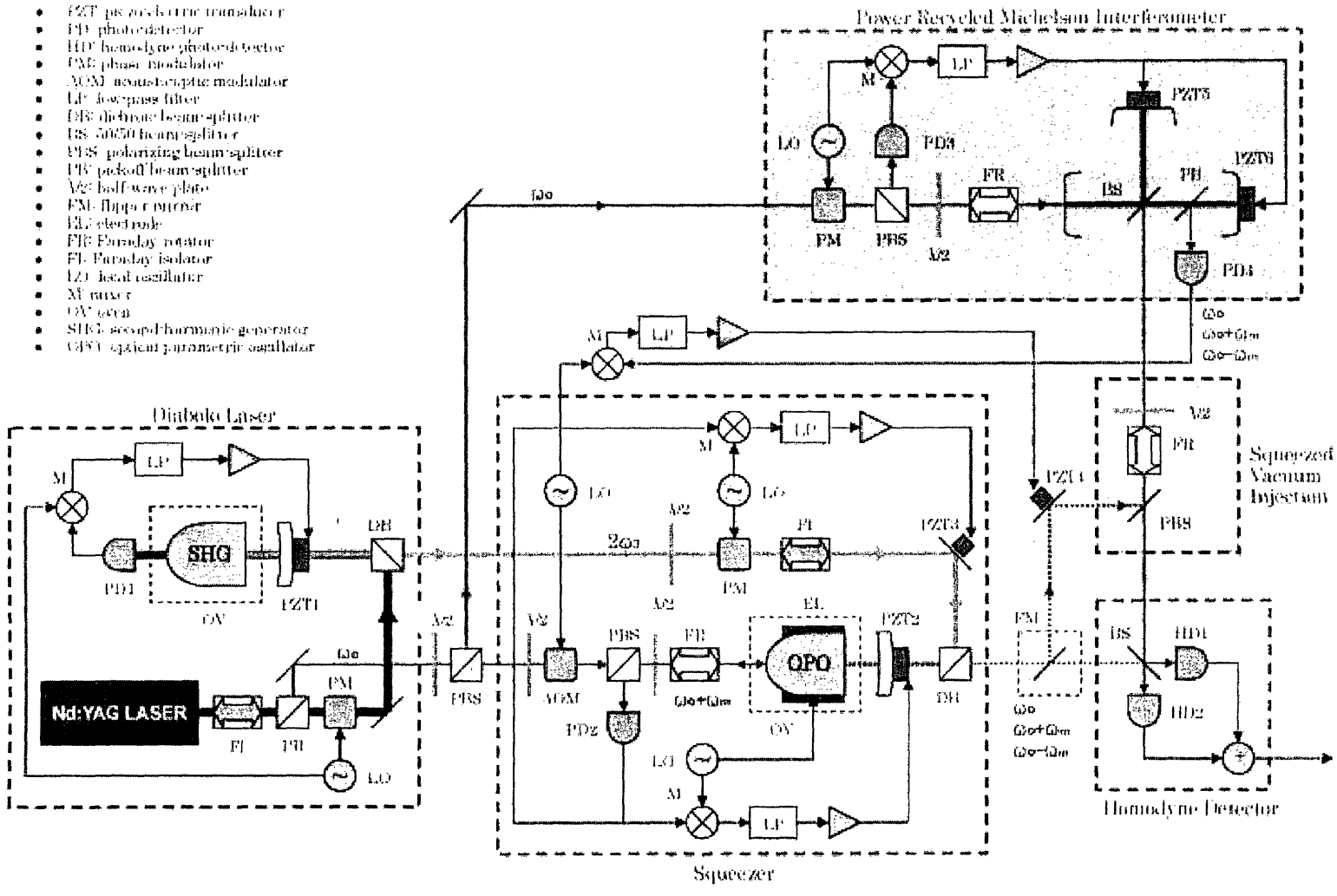

$a^\dagger$ is the annihilation operator for the beam at 1064nm.

$$\hat{H} = \hbar\kappa\beta_p(a^{\dagger 2}e^{-\imath\phi} + a^2 e^{\imath\phi}) \tag{2.1}$$

where β_p is the real amplitude of the pump beam, ϕ_p is the phase of the pump beam, and κ is a coupling constant that depends upon the nonlinear properties of the crystal.. The time evolution of a and $a^\dagger$ are given by Eqs. 2.2a and 2.2b.

$$\dot{a} = -\imath\Omega_p a^\dagger e^{-\imath\phi} \tag{2.2a}$$

$$\dot{a^\dagger} = \imath\Omega_p a e^{-\imath\phi} \tag{2.2b}$$

where $\Omega_p = 2\kappa\beta_p$. Eqs. 2.2a and 2.2b can be solved to yield the time dependence of a and $a^\dagger$.

$$a(t) = a_0 \cosh(\Omega_p t) - \imath a_0^\dagger \sinh(\Omega_p t) \tag{2.3a}$$

$$a^\dagger(t) = a_0^\dagger \cosh(\Omega_p t) + \imath a_0 \sinh(\Omega_p t) \tag{2.3b}$$

where $a_0 = a(0)$. a and $a^\dagger$ are directly related to X_1 and X_2, the quadratures of the generated beam; $X_1 = (a + a^\dagger)/2$ and $X_2 = (a - a^\dagger)/2\imath$. The variance of X_1 and X_2 are given by Eqs. 2.4a and 2.4b.

$$(\Delta X_1)_t^2 = \frac{1}{4}e^{-2\Omega_p t} \tag{2.4a}$$

$$(\Delta X_2)_t^2 = \frac{1}{4}e^{2\Omega_p t} \tag{2.4b}$$

Thus, an OPO can create a output beam that is 100% squeezed.

2.2 Detection of Squeezed Light

The detection of squeezed light requires specialized techniques and detectors. Vacuum squeezed light cannot be directly detected because it has no coherent amplitude. Vacuum squeezed states can be detected through the use of balanced homodyne de-

tection; the squeezed vacuum is combined with a local oscillator beam. The resulting beats can be seen at the homodyne detector.

2.2.1 Balanced Homodyne Detection

Balanced homodyne detection uses a reference beam that is phase locked to the input beam to provide a reference for the phase of the light; homodyne detection is able to differentiate between the two quadratures. The homodyne detection is balanced due

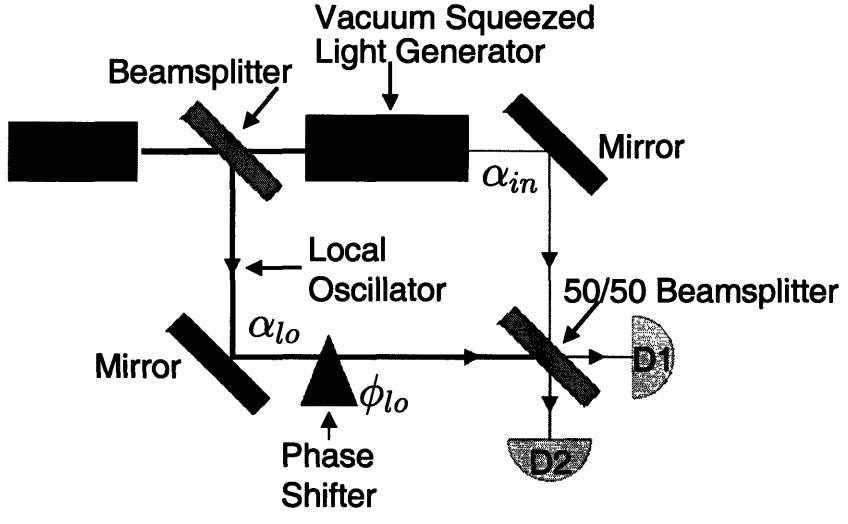

Figure 2-1 Balanced homodyne detection system. Note that the squeezed vacuum generator is a black box representation of the components used to create vacuum squeezed light. See Figure 2 for the full experimental apparatus. Taken from [2].

to the use of a 50-50 beam splitter that divides the incoming light into two beams of equal light power. The light power is then detected by two matched photodetectors. The difference current from the two detectors yields information about the phase of the squeezed vacuum.

$$i_{-}(t) \approx 2\alpha_{lo}(\delta X1_{in}(t)\cos(\phi_{lo}) + i\delta X2_{in}(t)\sin(\phi_{lo}) \tag{2.5}$$

where α_{lo} is the field of the local oscillator and ϕ_{lo} is the phase of the local oscillator. While the difference current is directly related to the amplitude of the local oscillator, the noise in the signal is due to the squeezed vacuum, and not the fluctuations of the

local oscillator. However, the power of the local oscillator must be much larger than that of the squeezed vacuum for this approximation for the difference current to be valid. The variance in the difference current, the quantity that is measured by a spectrum analyzer, is given by:

$$\Delta i_-^2 \approx 4\alpha_{lo}^2(\delta X1_{in}^2 \cos^2(\phi_{lo}) + i\delta X2_{in}^2 \sin^2(\phi_{lo}) \tag{2.6}$$

2.2.2 Effects of Quantum Efficiency

In the calculations performed so far, we have assumed that the photodetectors have a quantum efficiency of 1; every photon that hits the photodiode is converted into an electron [3]. Consequently, the spectrum of the current perfectly represents the spectrum of the incident light. However, no photodiode has a quantum efficiency, η, of 100%. For photodiodes with an incident light wavelength of 1064nm, the highest quantum efficiency photodiode, as reported by specification sheets is the EPITAXX ETX-500, which has a quantum efficiency of 95%. A list of other photodiode with high quantum efficiency at 1064nm is given in Table 3.1 in Chapter 3. A real detector can be modeled as a beamsplitter with transmission η followed by a detector with

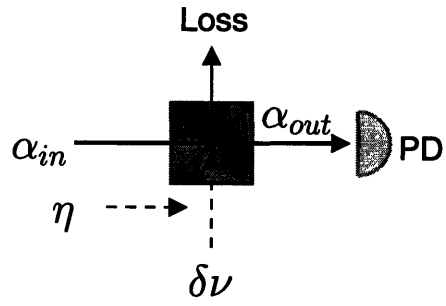

Figure 2-2 Detection with a photodetector of quantum efficiency η. Taken from [3].

η=1, as shown in Figure 2-2.

$$\alpha_{out} = \sqrt{\eta}\alpha_{in} + \sqrt{1-\eta}\delta\nu \tag{2.7}$$

The current is given by Eq. 2.7 times its complex conjugate, yielding:

$$I = \eta\alpha^2 + \sqrt{\eta}\alpha\sqrt{\eta}\delta X_{\alpha_{in}} + \sqrt{1-\eta}\delta X_{nu}) \tag{2.8}$$

where $\delta X_{\alpha_{in}}$ are the fluctuations in the input field and δX_{nu} are the fluctuations in the quantum vacuum introduced due to the lossy beamsplitter. The fluctuations of the quantum vacuum are just 1, the definition of the SQL. The variance in the photocurrent, V_I, is then given by Eq. 2.9.

$$V_I = N\alpha^2[\eta V_{\alpha_{in}} + (1-\eta)] \tag{2.9}$$

where $V_{\alpha_{in}}$ is the variance in the input of the fluctuation in the input field α_{in}. Dividing Eq. 2.9 yields a result normalized to the QNL.

$$V_I^{norm} = \eta V_{\alpha_{in}} + (1-\eta) \tag{2.10}$$

The importance of a high quantum efficiency is immediately seen; the quantum efficiency of the photodetectors sets the limit for the maximum amount squeezing that will be detected, no matter how much squeezing is produced.

Chapter 3

Low Noise, High Bandwidth Photodetectors

The stringent performance requirements on noise, quantum efficiency, and bandwidth control the design of the photodetectors. First, the detector must be shot noise limited to ensure efficient squeezing detection. Secondly, the detectors must employ a high quantum efficiency photodiode to prevent signal losses in the detection process. Finally, the detectors need a high bandwidth to yield the following signals: a DC signal for alignment, a 200Hz-1MHz band for squeezing measurements, and a side band detector at $\approx$ 10MHz that provides the error signal for locking of the homodyne detection system via Pound-Drever-Hall locking [6].

The homodyne detectors consist of five parts: the photodiode used to convert light into current, the bias circuitry used to maintain a constant reverse bias voltage across the photodiode, a resistor used to convert the photodiode current into voltage, a tuned circuit for the sideband detection, and a broadband detector with a range of DC-1MHz., as shown in the block diagram, Figure 3-1. Due to the time limitations and the complications involved with the design of RF circuitry, we chose to base the design for the homodyne detector upon an existing LIGO photodetector design. These LIGO photodetectors are used to detect light coming out the dark port of the LIGO interferometers; it has both a tunable RF output and a DC output capable of broadband detection. The design based on the LIGO photodetectors is located in

Appendix D.

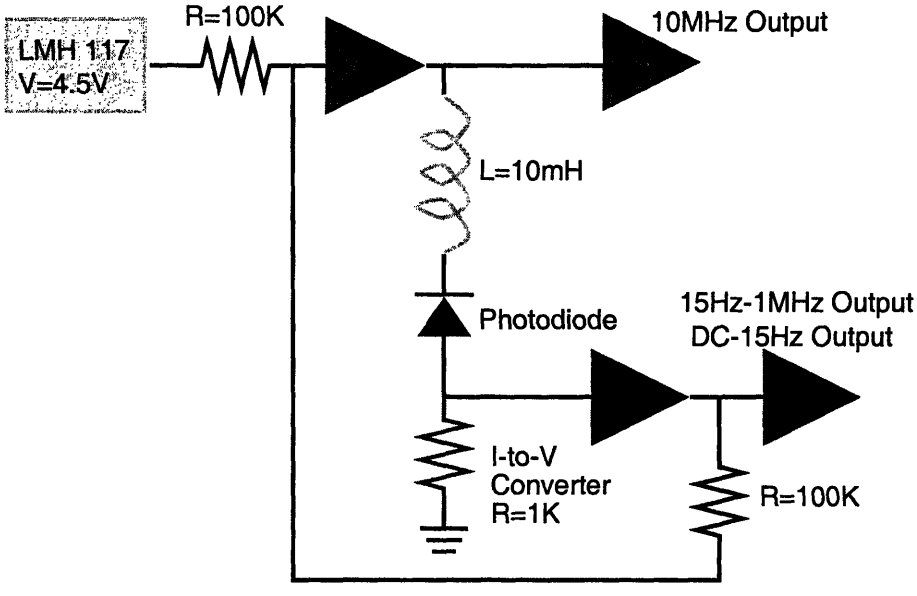

Figure 3-1 Block Diagram for Homodyne Detector

3.1 Photodiode Limitations

The photodiode is the first element of the homodyne detector; it detects the incident light and converts the signal into an electrical current [10]. We considered the following four factors in the search for the optimum photodiode: the quantum efficiency (η) at 1064 nm, the capacitance of the photodiode at a reverse bias of 5 V, the breakdown reverse bias voltage, and the minimum output current at 10mW, the expected operating light intensity. A list of photodiodes considered along with the four properties considered is given in Table 3.1.

The quantum efficiency of a photodiode is defined as

$$\eta = \frac{\text{number of electrons created}}{\text{number of incoming photons}} \tag{3.1}$$

This qualitative definition can be rewritten in terms of known variables, the incident power, P_0, the photocurrent produced, I, the wavelength of the incoming light, λ,

and physical constants, c, e, and h.

$$\eta = \frac{I}{P_0}\frac{hc}{e\lambda} = \frac{I}{P_0} \times 1.165 \tag{3.2}$$

A photodiode with a high quantum efficiency is desired in order to prevent losses in the detection of squeezed light.

The capacitance of the photodiode is another important consideration in the design process. If the capacitance of the photodiode is too large, the photodiode will limit the speed of the circuit. The capacitance of the photodiode forms an RC circuit with the 1 KΩ resistor that serves as the I-to-V converter[1]. If the capacitance is greater that 160pF, the broadband detector will have a 3dB bandwidth of less than 1MHz. However, there are other capacitors present in the circuit for the LC resonator at 10 MHz; consequently, the capacitance of the photodiode should be 70pF or less. The constraints on the size of the capacitance of the photodiode also limit the size of the photodiode; as the size of the photodiode increases, the capacitance increases. However, smaller photodiodes have some disadvantages; they require careful alignment due to the small active area of $1mm^2$ or less.

The relationship between reverse bias and capacitance is also a factor; due to limitations of the circuit, the maximum reverse bias that can be achieved when operating at 10mW light intensity is 5V. Also, the maximum reverse bias of the photodiode must be considered due to the bias circuitry incorporated into the photodiode circuit. If the photodiode can withstand a reverse bias greater than 15V, there would be no need to include the bias circuitry, leading to a simpler circuit.

Finally, the maximum output current of the photodiode is a consideration because the incoming light has a power of 10mW. If the photodiode cannot produce at least 10mA of output current, it will not fit the design criteria. After careful consideration, we chose to use the Perkins-Elmer C30641, a 1mm photodiode with an advertised quantum efficiency of 93%.

A list of the photodiodes considered, along with their size, quantum efficiency,

[1]The considerations that led to a choice of a 1KΩ resistor for the I-to-V converter will be discussed in Section 3.2.

Table 3.1. Photodiode Specifications.

Photodiode	Size (mm)	η %	Capacitance [2] (pF)	Maximum Reverse Bias (V)	Maximum Output Current (mA)
Perkins Elmer C30641	1	93	40	15	100
Perkins Elmer C30642	2	93	85	15	100
Hamamatsu G5832-2	2	93	300	15	175
GPD GAP2000	2	85	135	3	10

capacitance, reverse bias breakdown voltage, and maximum output current is listed in Table 3.1.

3.2 Shot Noise Limitations

As previously stated, during normal operation, 10mW of light at 1064 nm are expected upon each detector. Assuming a quantum efficiency of 100%, 10mW will yield a photocurrent of 8.6mA. From the equation for shot noise in a photodiode, which is derived in Appendix A,

$$i_{SN} = \sqrt{2 I_{DC} e} \tag{3.3}$$

where i_{SN} is the shot noise, I_{DC} is the DC current, and e is the charge of the electron, an 8.6mA current will yield a shot noise of $52.4 \frac{pA}{\sqrt{Hz}}$. A good requirement for a detector to be shot limited is that the electronic noise, Johnson noise and amplifier noise, should be $\frac{1}{10}$ of the shot noise, or 5.2 $\frac{nV}{\sqrt{Hz}}$. This calculation immediately determines the minimum size of the resistor used to convert the photocurrent into a voltage; the Johnson noise must be less than 5.2 $\frac{nV}{\sqrt{Hz}}$, which corresponds to a resistance of 603 Ω. As derived in Appendix B, the Johnson noise of a resistor is given by Eq. 3.4.

$$I_J = \sqrt{\frac{4kT}{R}} \tag{3.4}$$

I_J is the corresponding noise current, k is Boltzmann's constant, T is the temperature in K, and R is the resistance of the resistor in Ω. However, amplifiers are also present

in this circuit, which will cause more noise. The noise in amplifiers is discussed in Appendix C. Thus, we chose to use a 1 $k\Omega$ resistor for the I-to-V converter to allow for room in the noise budget for amplifiers in the DC-RF stage. In addition, most amplifiers running off 15V supplies have an output range between 11V and 12V; a larger resistor would have saturated the amplifiers.

We chose to use a resistor for the I-to-V converter due to both bandwidth and noise considerations. A transresistance amplifier is an inverting amplifier configuration, which leads to additional noise[3]. A transresistance amplifier also leads to bandwidth issues; creating a stable configuration while maintaining the high bandwidth would have required more complex circuitry. The capacitance of the photodiode combined with the resistance of the feedback resistor leads to a lagging phase shift and instability. A compensation capacitor is then required across the feed back resistor to maintain stability at the cost of bandwidth; the capacitor forms a low-pass filter with the feedback resistor.

3.3 Bias Circuitry

Due to the voltage rating on the Perkins-Elmer photodiode, we chose to operate the photodiode at a reverse bias of 4.5V. In addition, the capacitance of the photodiode depends on the reverse bias. A smaller reverse bias would increase the capacitance and thus reduce both the frequency of the tuned circuit and the bandwidth of the DC to 1MHz output, violating the design criteria. As shown in Appendix D, the reverse bias across the photodiode is set by the LMH-117 voltage regulator; it produces 4.5V. The voltage from the regulator is added to the measured voltage across the I to V converter; each voltage passes along a 100KΩ resistor before being summed, which leads to the sum being equal to only half of the voltage across the photodiode. The voltage across the I to V converter is measured between the two unity gain output operational amplifiers in the DC path. The summed voltages enter the OPA547F operational amplifier, which has a gain of 2. The output from the OPA547F then

[3]A discussion of noise in amplifier and various amplifier configurations is given in Appendix C.

goes across the photodiode and the I to V converter.

3.4 RF Sideband Detection

A key element of the detector is the sideband detector, which provides the sensor signal for PDH locking of the homodyne detection system. As shown in Appendix D, the side band detector consists of a tuned circuit of inductors L1 and L2 and the capacitance of the photodiode. In addition, two blocking capacitors are placed in the DC path to reduce the resistance of the I-to-V converter at 10MHz, the resonant frequency of the tuned circuit. Reducing the resistance leads to a higher Q for the tuned circuit, where the Q of the circuit is a measure of the width of the resonance; higher Q's correspond to smaller resonance widths. The RF output consists of a low pass filter followed by a gain of 5 stage. A MAX4107 op-amp was used to ensure a bandwidth of about 80MHz, in order to accommodate a broad range of RF sideband frequencies.

3.5 DC-1MHz Detection

The DC-1MHz stage required a broadband detector with a 3dB bandwidth of 1MHz. Both the capacitance of the photodiode and the capacitance of the blocking capacitor act with the I-to-V conversion resistor to form a RC low-pass filter, as shown in Appendix D. The maximum allowable capacitance to maintain a 3dB bandwidth is 160pF, which limits the photodiode choices, as shown by the capacitance values in Table 3.1. Since we want the blocking capacitor to be as large as possible, in order to increase the Q of the tuned circuit, we chose the Perkins Elmer photodiode, since it had the highest quantum efficiency with the lowest capacitance. The remainder of the DC-1MHz detector consists of a two low noise unity gain stable op-amp, the LT1128, which buffers the output of the stage. The first op-amp provides a place to measure the output of the I-to-V converter, in order to adjust the bias. The second op-amp serves as a buffer for the output.

During the calibration of the photodetectors, we chose to split the DC-1MHz output into two outputs. The spectrum analyzer used for data analysis had a maximum DC input of 7V; the detectors have an output of $\approx$ 7.7V when 10mW of light is shined on the detectors. Thus, the photodetectors where creating too much DC voltage for the spectrum analyzer. We chose to insert a high pass filter with a breakpoint frequency at 15Hz between the second op-amp and the original DC output, creating a DC-15Hz output and a 15Hz-1MHz output, as shown in Appendix D.

Chapter 4

Experiment and Data

4.1 Quantum Efficiency

We began by measuring the quantum efficiency of the photodectors. We measured the voltage and power for a range from 0.5mW to 11mW in increments of about 5mW. Figures 4-1 and 4-2 show the fit of the data to find the quantum efficiency of the photodiodes used in PD1 and PD2. For the measurements of quantum efficiency, the I-to-V converter had a resistance value of 0.878kΩ, as opposed to the design value of 1kΩ. For all other measurements, $R_{PD1} = 995\Omega$ and $R_{PD2} = 992\Omega$. Both photodetectors exhibit a linear response with little saturation in the specified operation range, 0mW-10mW.

4.2 Noise Measurements

We used a ??? spectrum analyzer to take noise measurements. All measurements were taken with a RBW of 1KHz and an averaging factor of 60. Figure 4-3 shows the predicted dark noise and the measured dark noise for both detectors. The predicted dark noise was determined by modeling the circuit, minus the bias circuitry, in HSPICE. We also used the spectrum analyzer to measure the shot noise at 5mW and 10mW. The data is shown in Figure 4-4. At 10mW, the shot noise is $\approx$ 40dBm above the dark noise, which corresponds to the shot noise being a factor of 100 greater than

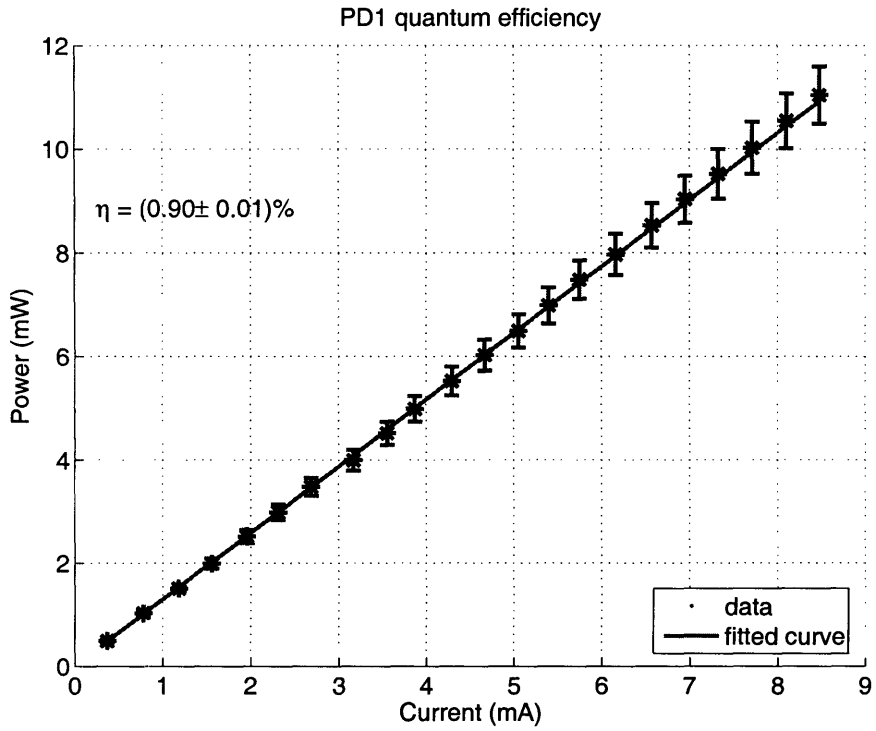

Figure 4-1 Quantum Efficiency of PD1

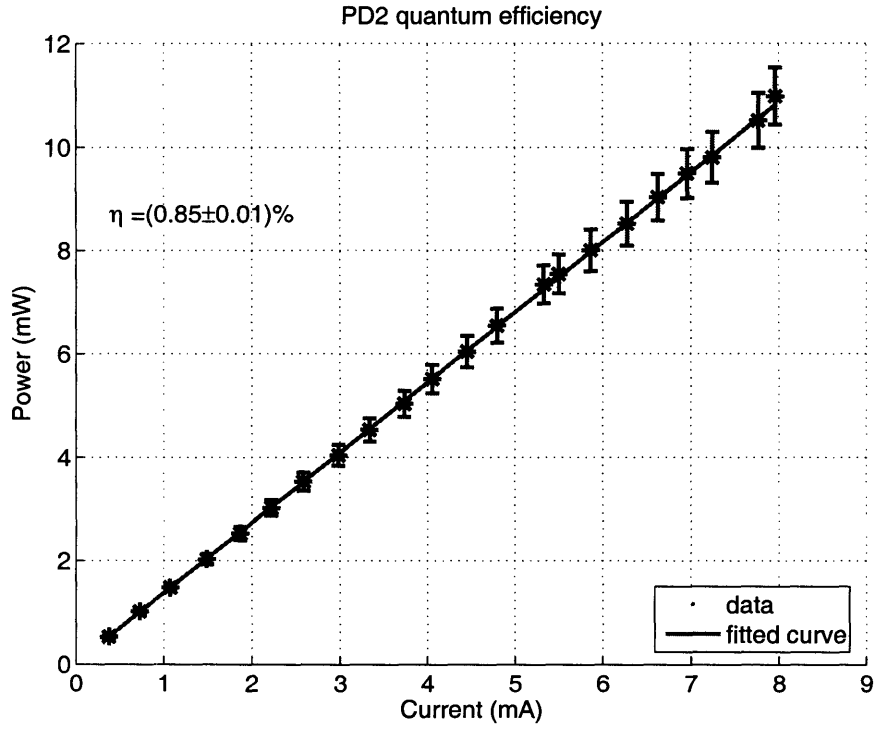

Figure 4-2 Quantum Efficiency of PD2

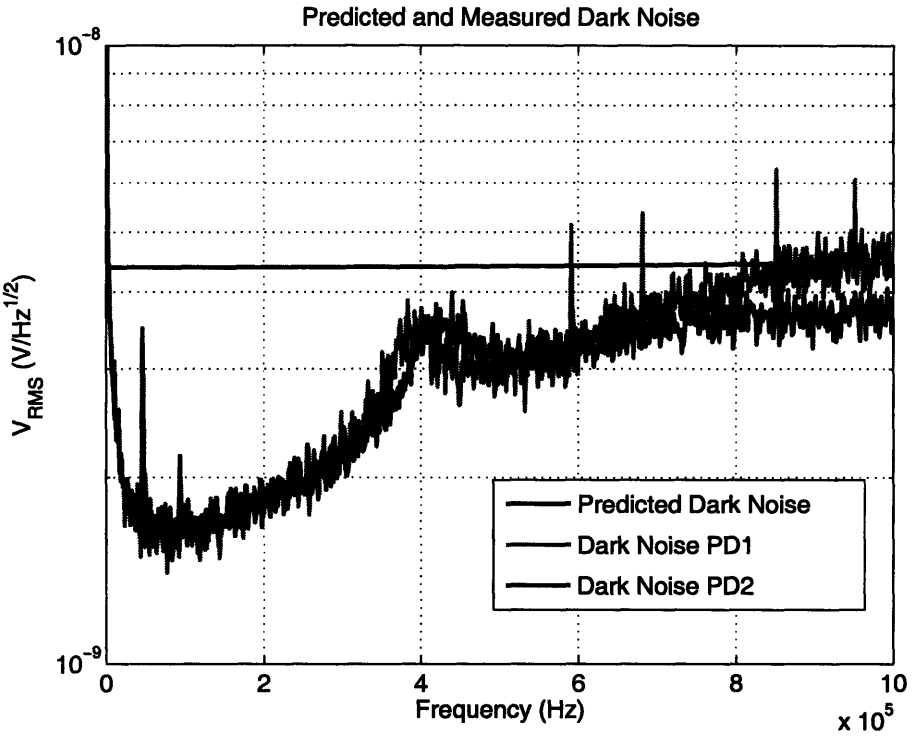

Figure 4-3 Predicted and Measured Dark Noise

the dark noise. Figure 4-4 also demonstrates that the frequency response remains relatively constant regardless of input power. The spikes in the lower frequency range for the shot noise at 10mW in PD2 were due to external noise sources. In addition, the frequency response of the photodetectors is closely matched, which will lead to more accurate squeezing measurements. Finally, we also measured the power at which the shot noise has the same value as the dark noise. We found that power to between 70 and 80 μV.

These photodetectors have a better quantum efficiency and are capable of detecting higher light power without saturation, such as the New Focus 1811 InGaAs photodetectors, as shown in Table 4.2.

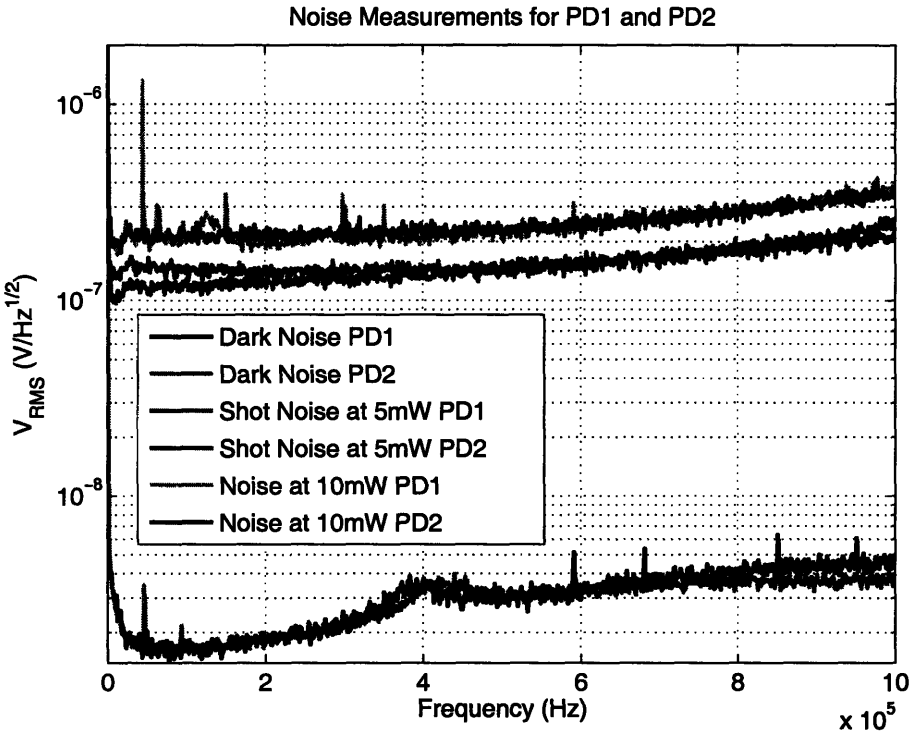

Figure 4-4 Noise Measurements

4.3 Squeezing

Due a problem with the heater in the OPO cavity, we were unable to measure squeezing. However, we can use Eq. 2.10 from Chapter 2 to determine how much squeezing we would have seen.

$$V_I^{norm} = \eta V_{\alpha_{in}} + (1 - \eta) \tag{4.1}$$

-2.5dB of squeezing was measured with the New Focus 1811 photodetectors. However, the New Focus 1811 photodetectors are prone to saturation above 1mW, which

Table 4.1. Photodetector Comparison.

Photodetector	*eta* %	Gain ($\frac{V}{mA}$)	Dark Noise at 1MHz ($\frac{V}{\sqrt{Hz}}$)	Maximum Input Power (mW)	3dB Bandwidth
New Focus 1811[1]	≈57	40	5.9×10^{-3}	1	DC-125MHz
PD1 and PD2	≈90	1	4.4×10^{-9}	≈13	15Hz-1MHz

leads to an estimated quantum efficiency of 57% for the squeezing measurement. If we assume that there were no other losses in the homodyne detector,[2] we can infer that the level of squeezing out of the OPO was about -6dB. Ignoring the sources of loss noted earlier, we would have seen about -4.8dB of squeezing, almost twice the amount seen by the New Focus 1811 photodetectors. Figure 4-5 shows a squeezing measurement made with the New Focus 1811 photodetecotrs.

[2]Due to a Faraday isolator with a 90% transmission efficiency and imperfect mode matching, there were quite likely more losses in the detection chain.

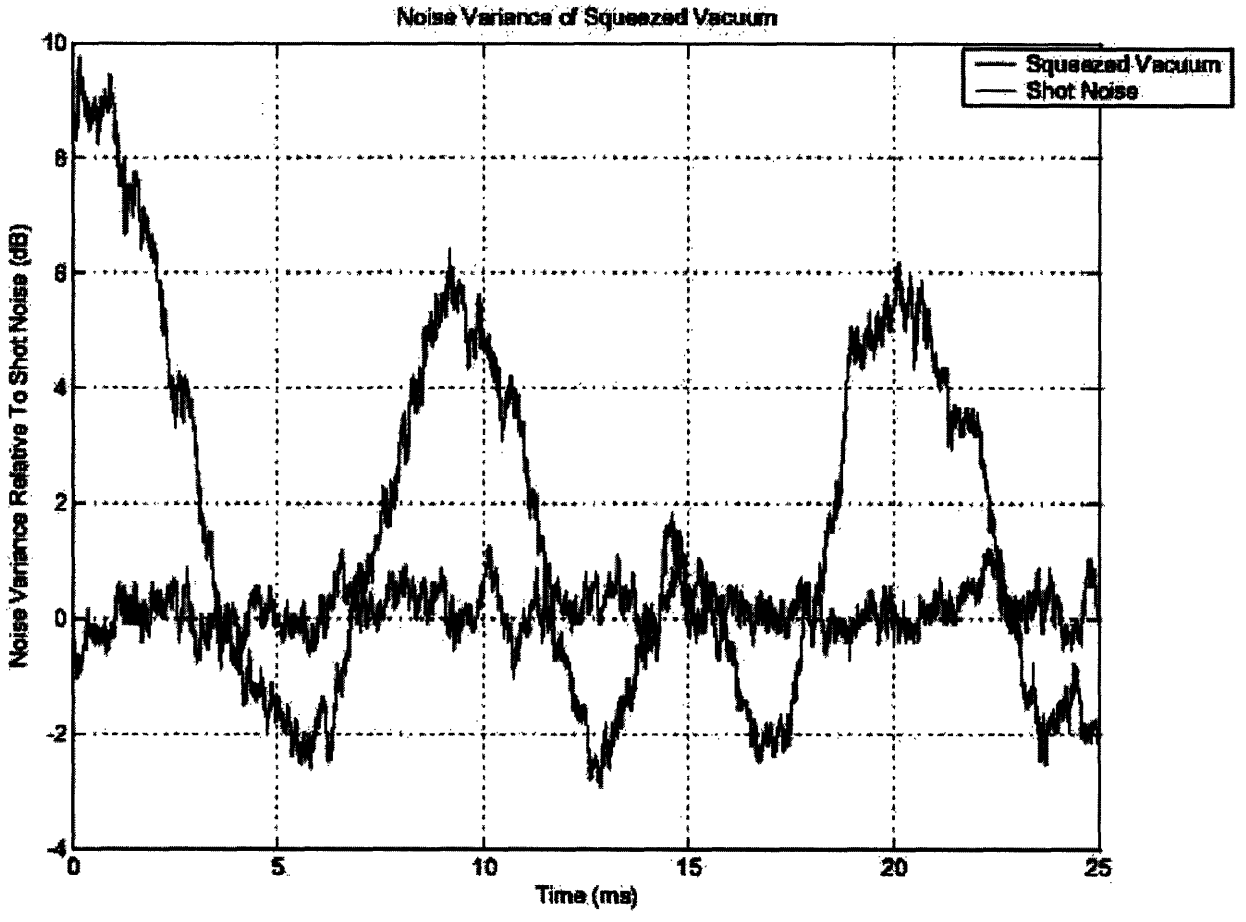

Figure 4-5 Squeezing measured with New Focus 1811 photodetectors

Chapter 5

Results and Conclusions

We have demonstrated that PD1 and PD2 have quantum efficiencies of $\approx 90\%$ and dark noise powers of about $4.4 \times 10^{-9} \frac{V}{\sqrt{Hz}}$. In addition, each photodetector can handle 10mW of power and is capable of detecting 0.55 of squeezed light.

Future improvements to the experiment include the use of photodiodes with the same quantum efficiency, as well as photodiodes with a slightly higher quantum efficiency. Future detectors will also need to handle more power while maintaining a low dark noise.

Appendix A

Shot Noise

Shot noise is a direct result of the quantization of electric charge. Following Stratonovich [13], each electric charge can be considered a pulse. However, each pulse is very small, so each charge can be represented by a delta function. The sum of the charges yields the total current:

$$I(t) = q\sum_{m}\delta(t - t_m) \tag{A.1}$$

where q is the charge of the electron. The current fluctuates around some average value, $I_{av} = \frac{Nq}{T}$, where N is the number of charges that pass through the current in some long time T. I_{av} and $\langle I^2 \rangle$ are related by the power spectral density, $S(f)$:

$$S(f) = \frac{\langle I^2 \rangle}{\Delta f} = 2\int_{-\infty}^{\infty} R(t')e^{-i2\pi f t'}dt' \tag{A.2}$$

where Δf is a unit frequency interval and $R(t')$ is the autocorrelation function. $S(f)$ is equal to twice the Fourier transform of $R(t')$, which relates the current at two different times separated by t'. The factor of 2 arises because $S(f)$ covers both negative and positive frequencies; only frequencies greater than 0 are of interest in this case, so only $\frac{1}{2}$ of $S(f)$ is used. The autocorrelation function is given by

$$R(t') = \lim_{T\to\infty}\frac{1}{T}\int_{-T/2}^{T/2} I(t)I(t + t')dt \tag{A.3a}$$

$$R(t') = \lim_{T\to\infty} \frac{q^2}{T} \sum_k \sum_{k'} \delta(t_k - t_{k'} + t') \tag{A.3b}$$

Eq. A.3a reduces to Eq A.3b after the definition of I(t) is substituted in. When $t_k = t'_k$, Eq. A.3b reduces to $I_{av} q \delta(t')$. When $t_k \neq t'_k$, the random phase of the argument of the delta function averages out over the total sum and makes no contribution. The Fourier transform of $qI_{av}\delta(t')$ is qI_{av}. Eq. A.2 reduces to

$$\frac{\langle I^2 \rangle}{\Delta f} = 2qI_{av} \tag{A.4}$$

Appendix B

Johnson Noise

Johnson noise is a result of thermal excitations of the modes of an electromagnetic field surrounding a conductor. However, summing up the energy in each mode for a conductor of arbitrary shape and composition is not practical. Following Nyquist [11], the problem can be reduced to one of finding the energy in the various modes of a transmission line. As shown in Figure B-1, two conductors of resistance R are

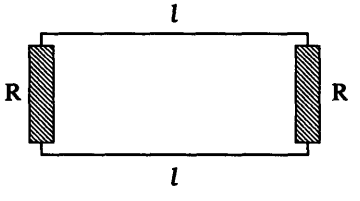

Figure B-1 Two conductors of resistance R connected by transmission lines of length l.

connected by a length of transmission line l, with impedance R. The system is in thermal equilibrium; consequently, the thermal excitation of the conductors and the resulting emf depends only upon frequency, resistance, and temperature. When the system is in thermal equilibrium, equal amounts of energy travel from one conductor to the other and vice versa. The line is subsequently isolated from the conductors; this situation is equivalent to that of a transmission line vibrating at its natural frequencies, given by $f = \frac{nv}{2l}$, where v is the velocity of propagation of the signal and n is an integer ≥ 1. The density of frequencies between frequencies f and $f + df$

is $D(f) = \frac{2ldf}{v}$. The average energy of any mode is kT; the electric field and the magnetic field each contribute $\frac{1}{2}k$T to the energy by the Equipartition Theorem. The energy can also be found from $\langle\epsilon(f)\rangle = \frac{hf}{e^{\frac{hf}{kT}}-1}$ which reduces to kT when $hf \ll k$T. The energy of the modes in that frequency range is

$$E(f) = D(f)\langle\epsilon(f)\rangle = \frac{2lkTdf}{v} \tag{B.1}$$

However, Eq. B.1 refers to the energy transmitted from one conductor to another and vice versa; only one of these transfers is under consideration. The power transfered from one conductor to the other during the time period $\frac{l}{v}$ with in the frequency range of interest is

$$P(f) = kTdf \tag{B.2}$$

The instantaneous power in the transmission line is related to the voltage across the line:

$$I = \frac{V}{2R} \tag{B.3a}$$

$$kTdf = \frac{dI^2R}{4R^2} = \frac{dV^2}{4R} \tag{B.3b}$$

Eqs. B.2 and B.3b can be combined to yield

$$dV^2 = 4RkTdf \tag{B.4}$$

Eq.B.4 can be rearragned to yield the relationship between the noise current due to Johnson noise and the resistance:

$$I_J = \sqrt{\frac{4kT}{R}} \tag{B.5}$$

Appendix C

Noise in Operational Amplifiers

Every operational amplifier has an intrinsic voltage noise, e_n, and an intrinsic current noise, i_n [9]. These intrinsic noises arise from the transistors that form the operational amplfier; these transistors have resistance that leads to Johnson noise and currents that lead to shot noise.[1] The equations that describe the input noise for an operational amplifier depends upon the configuration: inverting or non-inverting. The two configurations are shown in Fig. C-1. The noise for a noninverting amplifier includes

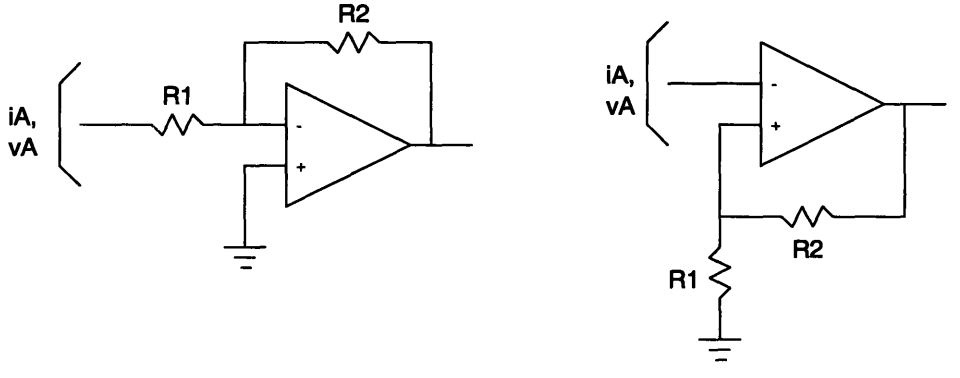

Figure C-1 Input Referred Noise in Amplifiers. Following [9].

both the intrinsic amplifier noise and the Johnson noise from the external resistors.

$$i_A^2 = i_n^2 \tag{C.1a}$$

[1]For a full discussion of operational ampplifiers and the noise sources in transistors, see [9], Chapters 3 and 7.

$$e_A^2 = e_n^2 + 4kTR_{||} + (i_n R_{||})^2 \tag{C.1b}$$

The noise for an inverting amplifier, such as a transresistance amplifier, has a different form for both current and voltage noise.

$$i_A^2 = i_n^2 + \frac{4kT}{R_2} \tag{C.2a}$$

$$e_A^2 = e_n^2 + (i_n R_1)^2 \tag{C.2b}$$

For comparison, the current and voltage noise for a resistor have the following equations:

$$i_R^2 = i_n^2 \tag{C.3a}$$

$$v_R^2 = 4kTR \tag{C.3b}$$

Appendix D

Schematic of Photodetectors

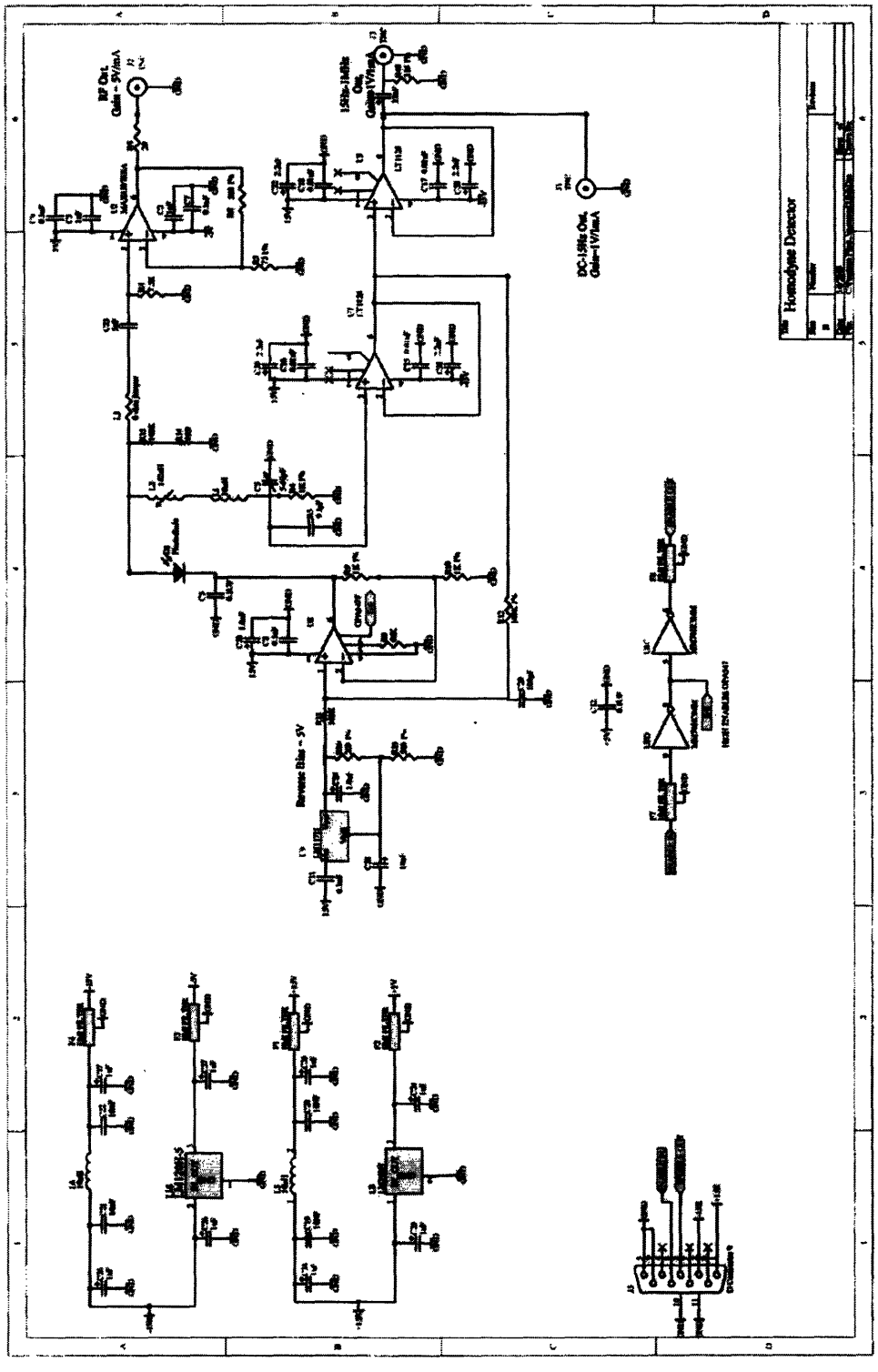

Figure D-1 Circuit Diagram for Photodetectors

Bibliography

[1] "A. Abramovici, W. Althouse, R. Drever, Y. Gursel, S. Kawamura, F. Raab, D. Shoemaker, L. Sievers, R. Spiro, K. Thorne, R. Vogt, R. Weiss, S. Whitcomb, , and M. Zucker. Ligo: The laser interferometer gravity-wave observatory. *Science*, 256:325–333, April 1992.

[2] Hans-A. Bachor and Timothy C. Ralph. *A Guide to Experiments in Quantum Optics.* Wiley-VCH, second edition, 2004.

[3] Benjamin Caird Buchler. *Electro-optic Control of Quantum Measurements.* PhD thesis, The Australian National University, 2001.

[4] Personal communication with Keisuke Goda.

[5] Thomas Corbitt and Nergis Mavalvala. Quantum noise in gravitational-wave interferometers. *J. Opt. B*, 6:S675–S683, 2004.

[6] R.W.P. Drever et al. Laser phase and frequency stabilization using an optical resonator. *Appl. Phys. B*, 31:93, 1983.

[7] Peter Fritschel. Second generation instruments for the laser interferomter gravitational observatory (ligo). In *SPIE Proceedings*, 2002.

[8] Osamu Hirota, editor. *Squeezed Light.* Elsevier, 1992.

[9] Paul Horiwitz and Winfield Hill. *The Art of Electronics.* Cambridge UP, 1989.

[10] Safa O. Kasap. *Optoelectronics and photonics: principles and practices.* Prentice Hall, 2001.

[11] H. Nyquist. Thermal agitation of electric charge in conductors. *Phys. Rev.*, 32:110–113, July 1928.

[12] Marlan O. Scully and M. Suhail Zubairy. *Quantum Optics.* UP, Cambridge, 1997.

[13] R.L. Stratonovich. *Topics in the Theory of Random Noise*, volume 1. Gordon and Breac, 1963.